Contrib. Astron. Obs. Skalnaté Pleso **56/1**, 156 – 185, (2026)
https://doi.org/10.31577/caosp.2026.56.1.156

Feeding frenzy in the mighty black holes: what we could learn from them

S. Panda[1], H. Benati Gonçalves[2], T. Storchi-Bergmann[2], M. Śniegowska[3], B. Czerny[4], E. Bon[5], P. Marziani[6], N. Bon[5], A. Rodríguez Ardila[7], D. May[1], M.A. Fonseca Faría[8], L. Fraga[8], F. Pozo Nuñez[9], E. Bañados[10], J. Heidt[11], K. Garnica[12] and D. Dultzin[12]

[1] *International Gemini Observatory/NSF NOIRLab, Casilla 603, La Serena, Chile, (E-mail: swayamtrupta.panda@noirlab.edu)*

[2] *Departamento de Astronomia, Instituto de Física, Universidade Federal do Rio Grande do Sul, CP 15051, 91501-970, Porto Alegre, RS, Brazil*

[3] *School of Physics and Astronomy, Tel Aviv University, Tel Aviv 69978, Israel*

[4] *Center for Theoretical Physics, Polish Academy of Sciences, Al. Lotników 32/46, 02-668 Warsaw, Poland*

[5] *Astronomical Observatory Belgrade, Volgina 7, 11060 Belgrade, Serbia*

[6] *INAF-Astronomical Observatory of Padova, Vicolo dell'Osservatorio, 5, 35122 Padova PD, Italy*

[7] *Observatório Nacional, Rua José Cristino, 77, São Cristovão, 20921-400, Rio de Janeiro, RJ, Brasil*

[8] *Laboratório Nacional de Astrofísica (LNA), Rua dos Estados Unidos 154, Bairro das Nações, Minas Gerais, Brazil*

[9] *Astroinformatics, Heidelberg Institute for Theoretical Studies, Schloss-Wolfsbrunnenweg 35, 69118 Heidelberg, Germany*

[10] *Max-Planck Institut für Astronomie, Königstuhl 17 Heidelberg, Germany*

[11] *Landessternwarte, Zentrum für Astronomie der Universität Heidelberg, Königstuhl 12, 69117 Heidelberg, Germany*

[12] *Universidad Nacional Autónoma de México, Instituto de Astronomía, AP 70-264, 04510, CDMX, Mexico*

Received: October 1, 2025; Accepted: November 20, 2025

Abstract. Eddington ratio ($\lambda_{\rm Edd}$) is a paramount parameter governing the accretion history and life cycles of Active Galactic Nuclei (AGNs). This short review presents a multi-faceted view of the importance of the Eddington ratio spanning varied AGN studies. We find that $\lambda_{\rm Edd}$ is crucial for standardizing the Radius-Luminosity (R-L) relation - a necessary step for employing quasars

(QSOs) as standardizable cosmological probes to help clarify the standing of the Hubble tension. In this data-driven era, we consolidated disparate aspects by developing novel relations borne out of large datasets, such as the robust, nearly *universal anti-correlation* between fractional variability (F_{var}) and λ_{Edd} derived from Zwicky Transient Facility (ZTF) data, which is vital for interpreting forthcoming high-cadence surveys like Rubin Observatory's LSST. Addressing the conundrum where JWST results suggest an overabundance of massive high-redshift black holes, we demonstrate that local AGNs offer clarification: Changing-Look AGNs (CLAGNs), driven by rapid λ_{Edd} shifts, cluster in the low-accretion regime ($\lambda_{Edd} \sim 0.01$), a rate independently confirmed by our integral field spectroscopy and photoionization modeling of a well-known Seyfert 2 galaxy, rich in high-ionization, forbidden, coronal lines. Conversely, for the high-redshift, high-luminosity population where traditional reverberation mapping (RM) is highly impractical, photometric reverberation mapping (PRM) offers a rapid alternative to constrain accretion disk sizes, enabling efficient estimates of black hole masses (M_{BH}) and λ_{Edd}. Finally, we developed tailored semi-empirical spectral energy distributions (SEDs) for extremely high-accretion quasars, successfully validating their characteristic extreme physical conditions.

Key words: supermassive black holes (1663) – active galactic nuclei (16) – quasars (1319) – spectroscopy (1558) – photometry (1234) – scaling relations (2031) – spectral energy distribution (2129) – photoionization (2060)

1. Accretion rate - a key parameter in AGN studies

The Black Hole Accretion Rate (BHAR) is among the fundamental properties that help define the state and activity of the central supermassive black hole (SMBH) residing at the very centers of galaxies. The BHAR or an equivalent parameter, the Eddington ratio, is the ratio of the net bolometric output from the active galactic nuclei (AGN) relative to the Eddington limit[1]. Coupled with the knowledge of the mass of the SMBH, the Eddington ratio enables an understanding of the accretion history and life cycles of AGNs (Netzer, 2015; Padovani et al., 2017; Alexander et al., 2025; Marziani et al., 2025). The applications of the Eddington ratio are far-fetched, from studying the temporal modulation of radiative output from individual AGNs to constraining the bulk-statistical growth of AGNs across cosmic time. It has been found to be a direct correlate to explain the dispersion in the well-known broad-line region (BLR) radius - AGN luminosity (R-L) relation (Martínez-Aldama et al., 2019; Du & Wang, 2019; Panda & Marziani, 2023). The R-L relation is an empirical scaling relation, where the BLR radius is estimated using the reverberation mapping (RM) technique, where one can estimate the excess in the light travel time between photons that directly arrive from the source of ionizing radiation (in the case of the SMBH, this is the accretion disk - a flattened disk-like structure arising

[1] $L_{Edd} \approx 1.26 \times 10^{38} \left(\frac{M_{BH}}{M_\odot}\right)$ erg s^{-1}.

from the loss of angular momentum as the matter accretes onto the SMBH), and those that get intervened by gaseous media in-between accretion disk and the distant observer before eventually making their way to the observer. This offset in the light travel time between the two (photon) paths helps determine how far the intervening, line-emitting media is from the source of the radiation. This intervening medium, in our case, is the broad-line region (BLR), which produces the bulk of the emission lines that we observe in an AGN spectrum due to a variety of radiative processes, e.g., recombination, collisional excitation, and fluorescence (Osterbrock & Ferland, 2006). We note, however, that the reverberation mapping technique has also been used to determine the sizes of the accretion disk itself (using the continuum reverberation mapping, Edelson et al. 2015), the sizes of the dusty regions (dust reverberation, Suganuma et al. 2006), and to map the further-out narrow-line region (NLR, Peterson et al. 2013).

Coming back to the R-L relation, having known the BLR radius, we now require the AGN luminosity. The general approach involves extracting the continuum flux from the AGN spectrum, wherein we look for narrow, line-free, continuum windows, and with an assumed cosmology, which gives us the luminosity distance, we can estimate the AGN luminosity. Therefore, having the AGN luminosity, for example, from a single-epoch spectrum, and with the aid of the R-L relation, we can infer the black hole masses using well-known scaling relations based on the virial theorem[2] and extends to the creation of large quasar catalogs (Marziani et al., 2003a; Vestergaard & Peterson, 2006; Shen et al., 2011; Panda et al., 2024a). This, then, allows us to get insight into the black hole mass distribution over a range of redshift and infer their activity with the combined knowledge of the black hole mass and the net bolometric output. Another advantage of the R-L relation has been to utilize it as, cosmologically speaking, a standardizable relation to infer the cosmology using quasars (Watson et al., 2011; Haas et al., 2011; Czerny et al., 2013). Here, we get the continuum flux as before, either through single epoch spectroscopy or carefully optimized photometry - either by a systematic modeling of the contaminants all except the accretion disk (Pozo Nuñez et al., 2023; Jaiswal et al., 2024), or through the usage of medium/narrow-band filters to avoid regions where such contributions from contaminants dominate (Chelouche et al., 2019; Panda et al., 2024b; Pozo Nuñez et al., 2025). Instead of assuming a cosmological model, we then perform the reverberation mapping to extract the size of the emitting region, here R_{BLR}, and infer the AGN luminosity using the R-L relation (Blandford & McKee, 1982; Peterson et al., 2004; Bentz et al., 2013; Panda et al., 2019a; Cackett et al., 2021). Having uniquely determined the continuum flux and the

[2]Here, the virial theorem requires the knowledge of the velocity dispersion (or FWHM) of a prominent emission line, its location (R_{BLR}) from the central gravitational potential, i.e., the SMBH, and the assumption of the geometry and distribution of the emitting gas around the SMBH. This latter term is usually referred to as the virial factor or f-factor (Collin et al., 2006; Panda et al., 2019b).

luminosity from independent methods, we can then derive the luminosity distance for each of these objects[3], and populate the Hubble-Lemaitre diagram and constrain the existing cosmological models. With the aid of quasars, we are well-poised to bridge the gap between the local and early Universe cosmological probes and help clarify the stance on the Hubble tension (Czerny et al., 2023a; Panda & Marziani, 2023; Di Valentino et al., 2025). However, to infer the Hubble constant, we aggregate the RM AGNs with other cosmological probes, e.g., Type-1 Supernovae, chronometric measurements of the Universe expansion, baryon acoustic oscillation data, quasar angular sizes, H II starburst galaxies, and Amati-correlated gamma-ray burst data (Cao et al., 2022; Czerny et al., 2023a). On the other hand, to get to the Hubble constant directly from AGNs alone, we need the aid of standard candles or standard rulers, e.g., the sizes of the accretion disks allow us to characterize the angular sizes of the AGNs, in conjunction with the redshift-independent luminosity distances (see e.g., Jaiswal et al., 2024).

A fundamental issue using the R-L relation has been the realization of the highly-accreting AGNs and their location on the R-L relation (Du et al., 2016; Grier et al., 2017; Du et al., 2018; Martínez-Aldama et al., 2019). When the R-L relation was first established, the scaling relation was built using multi-epoch, ground-based, and space-based spectrophotometric observations of well-known nearby Seyfert galaxies (Kaspi et al., 2000; Bentz et al., 2009). The slope of the relation was found to be close to the expectation from the standard photoionization theory, i.e., $\sim$0.5, especially after careful host subtraction (Wandel et al., 1999; Negrete et al., 2013; Panda, 2022). Fast forward to mid-2015, newer reverberation mapping (RM) campaigns, with luminous sources accreting at relatively higher rates albeit with lower variability amplitudes, started to populate a region in the R-L parameter space which demonstrated a significant dispersion from the existing R-L relation, thus giving rise to studies to understand what made these sources inherently different from their local counterparts (Du et al., 2018; Martínez-Aldama et al., 2019; Panda et al., 2019a). Later, in Martínez-Aldama et al. (2019), we found the key reason for the dispersion was directly connected to the Eddington ratio - the higher the value, the more the source deviates from the scaling relation, especially in the direction where the inferred R_{BLR} is shorter than expected. The problem, however, with the Eddington ratio in this context, is the way it is derived - the bolometric luminosity is derived from the continuum luminosity, and so is the black hole mass. This is the same luminosity that is the 'L' in the R-L relation, thus creating a circular loop. We need an independent observable that could trace the Eddington ratio. Many studies have pointed to the strength of the Fe II emission (or, R_{Fe}) to be a viable surrogate to the Eddington ratio through carefully statistical

[3]Given, $R_{BLR} \propto L^{0.5}$ from photoionization theory and the empirical R-L relation, and the AGN flux, $F = L/\ 4\pi d_L^2$, we can re-write luminosity distance, $d_L \propto R_{BLR}/\sqrt{4\pi F}$.

and theoretically-motivated studies (Sulentic et al., 2000; Marziani et al., 2003b; Marziani & Sulentic, 2014; Shen & Ho, 2014; Marziani et al., 2018; Panda et al., 2019b; Martínez-Aldama et al., 2021); c.f. Panda (2024) for a recent overview. Du & Wang (2019) (see also, Panda & Marziani 2023) eventually made the breakthrough, and provided us with an R_{Fe}-corrected R-L relation which not only solved the circularity problem, but brought the scatter in the newfound R-L to a measly 0.19 dex, re-instating the R-L relation as a standardizable relation for use in cosmology.

This is just one of the many highlights of the Eddington ratio and how it has come to the rescue. In later sections of this short contribution, we demonstrate a few recent studies that involve this key parameter and how it has helped improve our understanding of AGNs, and set the stage for the ongoing and upcoming, exciting studies with state-of-the-art facilities and observatories, e.g., JWST (Gardner et al., 2006), Dark Energy Spectroscopic Instrument (DESI, DESI Collaboration et al., 2025), and Rubin-LSST (Ivezić et al., 2019; Pozo Nuñez et al., 2023; Czerny et al., 2023b). In the following sections, we will summarize a few recent advancements that have allowed us to unravel the connection between the black hole activity and the mass of the SMBH, and in turn, the Eddington ratio, as well as the novel relations we have found. That would not be possible without the use of spectrophotometric observations of AGNs using a multitude of telescope facilities - targeted and survey-mode, single-epoch and monitoring campaigns, archival and new observations, covering the two hemispheres.

2. Getting ready for LSST: Photo-variability reveals a nearly Universal scaling relation

We have all been greeted with the *first look* of Rubin[4] and the potential it will have in the coming decade upon the start of its operations. We expect the Legacy Survey of Space and Time (LSST) to discover tens of millions of AGNs - a recent study of QSO number counts puts this to ∼12.2 million in i-band stretching to a 5σ median depth of 26.4 mag (Ivezić et al. 2019, Li et al., under review). The latest survey simulations (v5.0) suggest a mean cadence of nearly every half-night in *riz* bands in the Wide-Fast-Deep (WFD) mode, while this can be as high as every 3 nights for the u-band. The numbers are slightly more optimistic for the Deep-Drilling-Fields (DDFs, see e.g., Pozo Nuñez et al. 2024). The sheer amount of data that is going to be involved is nothing that we have analyzed before. Not to forget, it is going to be a daunting challenge to get a spectroscopic follow-up for all these detections, although some upcoming surveys seem promising (ESO/4MOST - de Jong et al. 2019; Frohmaier et al. 2025, SpecS5 - Besuner et al. 2025, WST - Mainieri et al. 2024). In anticipation of the start of Rubin operations and to tackle the prospective challenge of spectra-starving,

[4] https://rubinobservatory.org/gallery/collections/first-look-gallery

we looked into the large repository of photometrically detected and monitored AGNs in the Zwicky Transient Facility (ZTF, Bellm et al., 2019; Graham et al., 2019) that led to a rather convincing discovery.

2.1. Photometric variability anti-correlates with the Eddington ratio

The paper (Benati Gonçalves et al., 2025) presents a systematic study of optical variability for 915 type-1 quasars with $0 \leq z \leq 3$, using ZTF g-band light curves and Sloan Digital Sky Survey (SDSS) DR16 spectral parameters (including black-hole masses, bolometric luminosities, and Eddington ratios). These sources were pre-selected from the All Quasar Multiepoch Spectroscopy (AQMES) MEDIUM subsample of the Black Hole Mapper project of the SDSS-V (Kollmeier et al., 2019). We computed the fractional variability amplitude (F_{var}) via the excess-variance formalism, and after rigorous filtering (≥ 100 observations, $F_{var} > 0$) and correcting for minimal emission-line contributions (a few percent of the continuum flux), we arrive at a key result - a redshift-independent anti-correlation between F_{var} and the Eddington ratio (λ_{Edd}). The best-fit relation for the full sample is

$$\log \lambda_{Edd} = (-0.71 \pm 0.06) \log(F_{var}) - (1.52 \pm 0.06) \quad (1)$$

or equivalently $F_{var} \approx 10^{-0.71} \lambda_{Edd}^{-1.52}$ (see, e.g., Figure 1 for a revised version). This yields a Pearson coefficient r ≈ -0.31 ($p < 0.01$) for all redshifts, with the strongest anti-correlation at low-z (r ≈ -0.40) and a marginal trend in the highest bin ($2 \leq z < 3$). We present a general equation encapsulating this relationship, which appears to be almost free of redshift dependence, enabling predictions of quasar variability based on accretion parameters or vice versa, a significant enhancement to prior works (see e.g., Klimek et al., 2004). The derived relation with the Eddington ratio provides a unified framework for interpreting variability in AGNs and facilitates future studies of quasar variability using high-cadence surveys, such as the Vera C. Rubin Observatory's LSST (Ivezić et al., 2019).

Additional correlations show that F_{var} declines monotonically with continuum luminosities L_{1350}, L_{3000}, L_{5100}, and bolometric luminosity across all redshift bins (negative Pearson r values ranging from -0.23 to -0.59), while, the F_{var}–M_{BH} relationship evolves from a weak positive correlation at low-z (r ≈ 0.22) to a moderate anti-correlation at high-z (r ≈ -0.36). We discussed potential selection biases (luminosity-driven Malmquist bias, rest-frame time-baseline shortening at high-z) but demonstrate that the correlation between F_{var} and λ_{Edd} is largely free of any significant redshift dependence (see Benati Gonçalves et al., 2025, for more details).

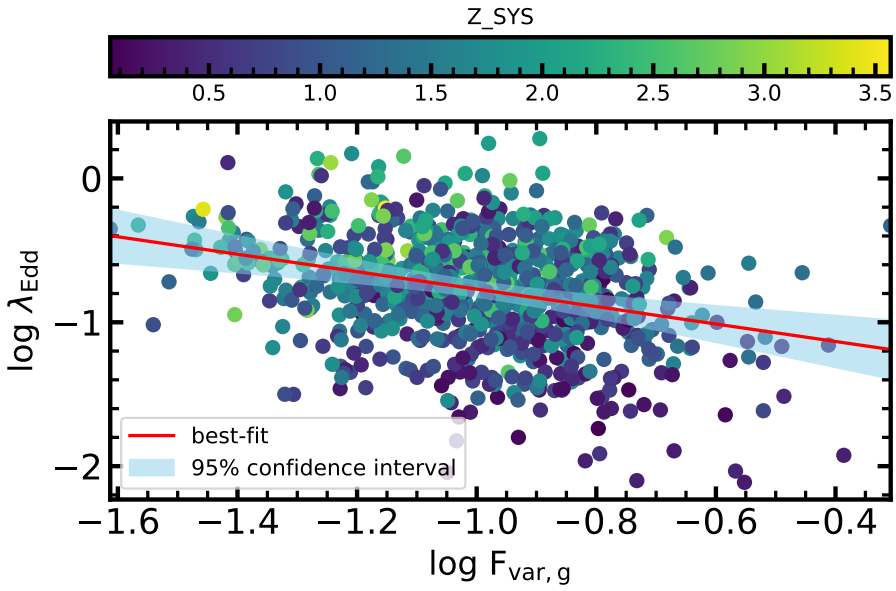

Figure 1. Distribution of the fractional variability (F_{var}) in the g-band ZTF lightcurves for the AQMES medium field monitored within the SDSS-V, versus the Eddington ratio. The latter is taken from the SDSS DR16 QSO catalogue (Wu & Shen, 2022). The color axis depicts the distribution of redshift. The best-fit correlation after cleaning sources with insufficient F_{var} in g-band information: log λ_{Edd} = -0.61 log F_{var} - 1.38 (ρ = -0.28; p-value = 2.8E-18).

2.2. Possible biases and streamlining the parent sample

Below, we summarize some additional tests of robustness for our newfound scaling relation.

– lightcurve baseline testing: as it currently stands, the correlation involves all AGNs with at least 100 observations in overa 6-year period (mid-2017 to late-2023). The median of the number of g-band observations is 304; thus, we attempted to check the correlation for only those cases where the number of visits was $\geq$ 300. We were left with 53% of the number of AGNs (488/920). However, the correlation grew stronger: log λ_{Edd} = -0.71 log F_{var} - 1.50 (ρ = -0.31; p-value = 2.74E-12), almost identical to the original version as shown in Eq. 1.

– removing host-dominated sources: Given the wide range of redshift considered in the sample selection (z $\leq$ 3), we decided to also check the variety in our sample with respect to the contamination induced by the presence

of a strong host component. This is especially an issue for the low-z sample ($z \leq 1$), where the fitting routine in the spectral decomposition code PyQSOFit (Guo et al., 2018) - the mainstay pipeline used to derive the SDSS DR16 QSO catalog chooses whether to fit a host-galaxy component to the spectrum or not, based on a minimum number of host-galaxy pixels identified by the routine. If this criterion is not met, no host galaxy component is fit. Another way to look at this issue is that if the AGN dominates the spectrum, the resulting fit will have a negligible host-galaxy contribution. At the moment of writing, we do not have a straightforward way to filter such sources out without this information. On the other hand, for the sources with $z > 1$, no host galaxy template is incorporated (the host galaxy template fits within the rest-frame SDSS range, i.e., 3450-8000 Å). Therefore, we only rely on the Malmquist bias for this latter case. Nonetheless, we made a simple test to account for the host contribution. The QSO catalog does provide us with the fractional host contribution at 5100Å ($f_{host,5100}$). We plotted the distribution for $f_{host,5100}$ and noted a clear dichotomy at 0.4 (see Figure 2 left panel). After filtering out the sources' significant host contribution (> 40%), resulting in recovery of 86% of the sample (792/920), we still recover a familiar version of the correlation between λ_{Edd} and F_{var}.

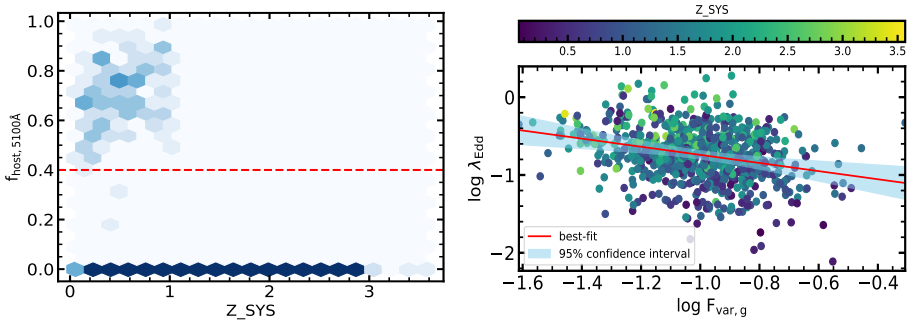

Figure 2. (Left:) Host fraction (estimated at 5100 Å) as a function of redshift for our sample. The hexagons highlight the number density of sources with a darker shade of blue corresponding to higher density. (Right:) The best-fit correlation after filtering out the sources with significant host contribution (>40%): log λ_{Edd} = -0.52 log F_{var} - 1.26 (ρ = -0.27; p-value = 7.1E-15).

– combining the above two cases: taking the two above cases together and making the cut, we recover a correlation similar to the original one (with 44% of the sample): log λ_{Edd} = -0.62 log F_{var} - 1.37 (ρ = -0.3; p-value = 9.78E-10).

– quality cut on the relative error in F_{var}: Next we capitalize on the relative error in the F_{var} itself. The $errF_{var}/F_{var}$ in the g-band has a distribution with a median around 57%. Thus, we tried a simple cut to limit to the sources with less than 50% in relative error in F_{var}. This led to a substantial reduction in the remaining sources (∼39%; 357/920). Applying this cut only, we get a stronger correlation than its original form: log λ_{Edd} = -0.83 log F_{var} - 1.54 (ρ = -0.32; p-value = 5.78E-10).

– dependence on the M_{BH} bins: To check the co-dependence of M_{BH} on the derived correlation, we made a test by binning the sources within 4 equal bins of M_{BH}. The M_{BH} distribution for the cleaned sample of 920 sources ranges from $10^{6.81}$ to $10^{10.32}$ $M_{\odot}$, with a mean $\sim 10^{8.99}$ $M_{\odot}$ (σ = 0.55 dex; median mass = $\sim 10^{9.09}$ $M_{\odot}$). We thus constructed 4 bins, each of 1 dex width, i.e., between 6.5 - 7.5, 7.5 - 8.5, 8.5 - 9.5, and 9.5 - 10.5. These bins have 14, 148, 607, and 151 sources, respectively. The correlation for each M_{BH} bin is found as follows:

  – bin-1: log λ_{Edd} = -0.79 log F_{var} - 1.53 (ρ = -0.1; p-value = 0.725)

  – bin-2: log λ_{Edd} = -1.03 log F_{var} - 1.71 (ρ = -0.47; p-value = 2.32E-09)

  – bin-3: log λ_{Edd} = -0.58 log F_{var} - 1.33 (ρ = -0.25; p-value = 7.97E-10)

  – bin-4: log λ_{Edd} = -0.65 log F_{var} - 1.54 (ρ = -0.38; p-value = 1.62E-06)

  Given that most of the sources (66%) are in bin-3, the resemblance of the correlation for this bin relative to the cleaned sample is expected. We note also the shifting range in the redshift range as we move along the M_{BH} bins, which is connected to the Malmquist bias (wherein we tend to observe the brighter targets as we transcend in redshift). Another reason is the sensitivity of our spectrograph detectors, which marks a limiting magnitude below which the detection of targets is seldom. Given the direct proportionality between the M_{BH} and luminosity, the faintness of the target could lead to the estimation of a lower M_{BH} for these sources. We, however, miss these sources as we go along the redshift. We, therefore, need better facilities (e.g., DESI; Pucha et al. 2025) to probe this low-luminosity regime, esp. in the higher z regime, to have a better handle on completeness of the sample.

  However, interestingly, the correlation for bin-2 (7.5 - 8.5) is found to be the strongest among all (ρ = -0.47 with a slope suggesting an almost 1-to-1 inverse relation between F_{var} and λ_{Edd}). The top panel of Figure 3 shows the consolidated version of each bin's performance. This reveals an interesting conclusion: the dispersion between the individual best-fits varies between ∼ 0.5 dex (for the smallest values of log F_{var}) to ∼ 0.25 dex (for the largest values of log F_{var}). These values are consistent with the dispersion in the M_{BH} scaling relations often adopted (e.g., the M-$\sigma_{\star}$ relation with a dispersion ∼0.44 dex, Prieto et al. 2022; and similarly for RM-derived M_{BH},

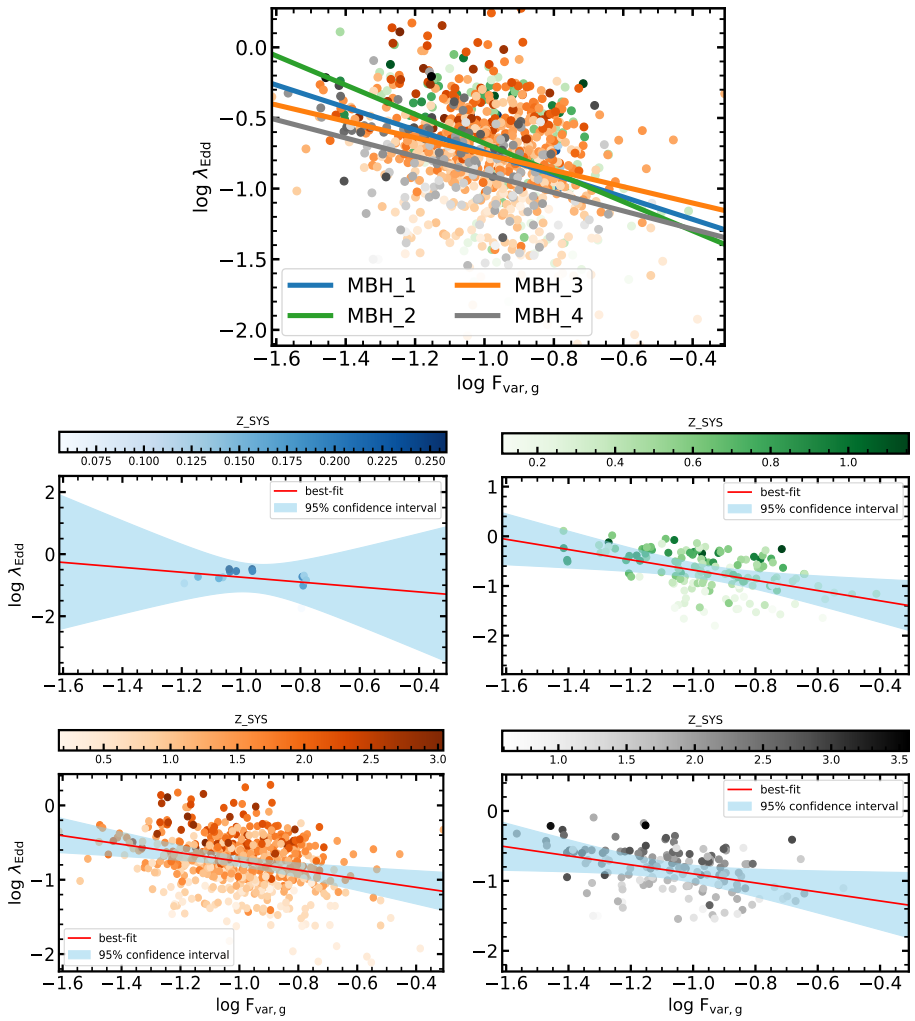

Figure 3. Correlations similar to as shown in Figure 1, but with the data binned in four separate bins of M_{BH} (in log-scale, in $M_{\odot}$ units): between 6.5 - 7.5 (blue), 7.5 - 8.5 (green), 8.5 - 9.5 (orange), and 9.5 - 10.5 (grey). The sources are colored as per their respective M_{BH} bins, while the gradient in color represents the corresponding range in redshift as depicted in the lower sub-panels. The best-fit per M_{BH} bin is shown in the top panel. Each of the lower sub-panels shows the individual best-fit to the binned data per M_{BH} bin. The color-axis in each of these sub-panels is the redshift corresponding to the respective bin. Note the shifting range in the redshift range as we move along the M_{BH} bins.

i.e., between 0.4 - 0.51 dex, Du & Wang 2019). Also, it is interesting to see that, apart from the M_{BH} bin containing the largest BH massed sources, the rest of the three relations coincide around log F_{var} $\sim$ -0.9 and log λ_{Edd} $\sim$ -0.75. This could suggest that the correlation briefly becomes independent of the M_{BH} variations within this region.

Overall, these experiments only reinforce the *almost* universality of the relation found between the fractional variability (F_{var}) and the Eddington ratio (λ_{Edd}). The derived universal F_{var}–λ_{Edd} relation, therefore, enables predictions of quasar variability from accretion parameters and vice versa, offering a powerful tool for upcoming high-cadence surveys.

3. Changing-look and how?

The last decade has seen a surge in the detections of changing-look AGNs (CLAGNs) - these sources have marked increases in their variability features compared to their counterparts, which we discussed in the previous section; thanks to massive, multiplex spectroscopic surveys such as SDSS and DESI, to name a few. Combination of intensive photometric monitoring, e.g., Catalina Real-Time Transient Survey (CRTS, Drake et al., 2009) and Zwicky Transient Facility (ZTF, Bellm et al., 2019; Graham et al., 2019) and multi-epoch spectroscopy have revealed $\geq$ 500 known CLAGNs to date (Temple et al., 2023; Wang et al., 2024; Zeltyn et al., 2024; Guo et al., 2025b). Many of these detections were serendipitous to start with, but as we prepare for Rubin LSST to start its operations, the community has become more aware of selection criteria to look for CLAGNs in massive datasets, and even forecast the changing-state of these AGNs (Graham et al., 2020; Sánchez-Sáez et al., 2021; Ricci & Trakhtenbrot, 2023). With the aid of beyond-meter class facilities, e.g., Gemini/ESO-VLT/DESI, we now peer deep into the redshift space to reveal CLAGN candidates close to the cosmic noon (Ross et al., 2020; Guo et al., 2025a). Understanding the nature of this special class of AGNs in contrast to the general variable nature of AGNs is vital to our understanding and perhaps aids in revealing new classes of CLAGNs, e.g., the extreme variability quasars (EVQs, Ren et al., 2022).

In this direction, we (Panda & Śniegowska, 2024) made a significant stride to reveal where the population of the CLAGNs is mostly discovered through a systematic analysis of known SDSS CLAGNs. In the next sub-section, we describe our methodology and the key findings that connect again the key parameter - Eddington ratio (see left panel in Figure 4).

3.1. Eddington ratio distribution as a proxy to catch Changing-Look AGNs

The paper by Panda & Śniegowska (2024) presents a homogeneous spectroscopic analysis of 93 CLAGNs compiled from the SDSS, BOSS, and eBOSS archives. Multi-epoch spectra are processed with the PyQSOFit pipeline (Guo et al., 2018), delivering epoch-resolved measurements of the AGN continuum, broad-line parameters, black-hole mass (M_{BH}), and Eddington ratio (λ_{Edd}). The sample was assembled by cross-matching existing CLAGN catalogs and retrieving all available SDSS spectra, ensuring at least two epochs with detectable broad Hβ emission profiles. Spectral decomposition follows the standard PyQSOFit methodology, incorporating a power-law continuum, Fe II emission templates, and host-galaxy eigenspectra when required. Each epoch is placed on the optical Eigenvector 1 (EV1) plane, i.e, the optical plane between the broad FWHM(Hβ) versus the strength of the optical Fe II emission, i.e., the parameter R_{Fe}. This is the canonical quasar main-sequence diagram (Boroson & Green, 1992; Sulentic et al., 2000; Marziani et al., 2001, 2018; Panda et al., 2019b; Panda, 2024). The majority of CL-AGNs evolve within Population-B (FWHM Hβ $>$ 4000 km/s), with only a few exhibiting inter-population transitions (A $\rightleftharpoons$ B). Turn-on events are accompanied by systematic shifts toward lower M_{BH} and, therefore, higher λ_{Edd}, supporting accretion-rate modulation as the primary driver of the phenomenon. We then classified the sources as "Turn-On", "Turn-Off" or mixed "On-Off" cycles; and found that the distribution is dominated by simple monotonic transitions, echoing earlier reports that turn-off events are more frequently observed (Shen & Burke, 2021). Balmer-decrement (Hα/Hβ) variability is examined for 32 objects with at least 3 epochs. The ratios display diverse temporal behavior, often deviating from the case-B value ($\sim$3.1, Osterbrock & Ferland 2006), implying a complex interplay among dust extinction, BLR density, and ionizing-continuum changes. The resulting database furnishes a comprehensive resource for probing the physical mechanisms behind AGN spectral variability. The systematic migration of CLAGNs on the EV1 and M_{BH} - λ_{Edd} planes bolsters models in which rapid accretion-rate fluctuations dominate the changing-look phenomenon (Noda & Done, 2018; Sniegowska et al., 2020), while heterogeneous Balmer-decrement trends suggest additional BLR structural evolution.

The main finding from this study was the realization of the Eddington ratio distribution of these CLAGNs. We specifically consider the spectral epochs as widely separated in time and with the most variation in the continuum and emission line characteristics to reveal that the CLAGNs dominate the low-accretion regime ($\lambda_{Edd} \sim 0.01$), dominated by sources in the Population B (FWHM H$\beta \geq$ 4000 km s^{-1}), in contrast to the high accretors that dominate the Population A parameter space (Du et al., 2018; Panda et al., 2019b; Śniegowska et al., 2021; Garnica et al., 2022).

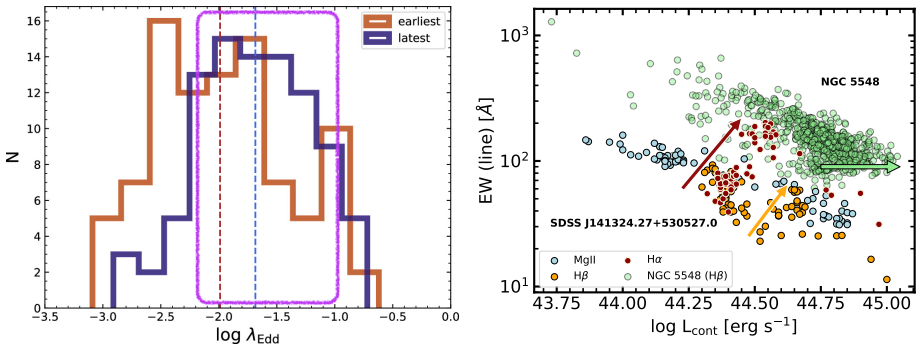

Figure 4. (*Left:*) Distribution of Eddington ratios in the sample from Panda & Śniegowska (2024). We show the distributions for the earliest (in brown) and the latest (in purple) epochs for the sources in our sample. The median values for the two distributions (red = -1.99, blue = -1.685) are marked with vertical dashed lines. The magenta box marks the range of the Eddington ratio for NGC 5548, i.e., log $\lambda_{\rm Edd}$ = [-2.2, -1]. (*Right:*) The distribution of the emission line EW versus the AGN continuum luminosity. Here, we demonstrate the trend for two sources: SDSS J141324.27+530527.0 (Wang et al., 2018) with 72 spectral epochs over ∼15 years (5527 days), and NGC 5548 (Bon et al., 2018; Panda et al., 2022, 2023) with more than 750 spectral epochs over ∼25 years (9624 days). For the former source (SDSS J141324.27+530527.0), we have taken the spectral data from the homogeneous fitting in Panda & Śniegowska (2024), which includes the MgII, Hβ, and Hα emission lines and the corresponding AGN continua nearest to these lines (at 3000Å, 5100Å, and 6000Å), as shown in the panel. For NGC 5548, we show the dataset from Panda et al. (in prep.), which is an updated version of the dataset provided in Bon et al. (2018), where the authors analyzed the Hβ region. The SDSS source shows a clear rise from a deep minimum to a high state in both Balmer lines. However, the MgII shows a rather flat behavior - reminiscent of the Baldwin effect, suggesting the difference in ionization and response to the changing continuum levels. NGC 5548 data has a wealth of data, but the change in the source is rather gradual, and hence, a clear spike in the trend is not that prominent.

3.2. Population studies vs. tracking the changes in an individual source

Going back to the BLR structural evolution, it would be great if we could capitalize on single-object studies over longer temporal baselines to reveal and distinguish between short, intermediate, and long-term variations in these AGNs. We are fortunate to have such rich datasets focused on single AGN spectrophotometric monitoring, notably of the prototypical Population B source - NGC 5548. Taking advantage of $\geq$ 30 years of data compiled from $\sim$ 17 individual observing campaigns - including the AGN Watch and AGN STORM projects (Peterson et al., 2002; Shapovalova et al., 2004; De Rosa et al., 2015; Fausnaugh

et al., 2016; Pei et al., 2017), we (Panda et al., 2022, 2023) re-discovered the saturation of the Hβ emission with growing AGN continuum luminosity, also known as the Pronik-Chuvaev effect (Pronik & Chuvaev, 1972). NGC 5548 has telltale signatures of being a CLAGN, and this anomalous behavior of the Hβ with changing continuum luminosity (Gaskell et al., 2021) has opened new avenues for us to improve our spectral models to not only reveal the inner working of the AGN, but to use this source as a laboratory to better understand the CLAGN behavior. For instance, in the right panel of Figure 4, we demonstrate the trend between the EW(Hβ) with increasing AGN luminosity, the well-known Baldwin effect (Wandel, 1999; Martínez-Aldama et al., 2021) - however, we see a flattened behavior at the extreme high end of the luminosity. This is the Pronik-Chuvaev effect. We try to check whether the CLAGNs that were studied in Panda & Śniegowska (2024) show a similar behavior to NGC 5548. To this end, we consider our best case - SDSS J141324.27+530527.0 (Wang et al., 2018), an object with 72 spectral epochs spanning over ∼15 years (5527 days). Another interesting thing with the latter source is the availability of EW information for Mg II, and Hα, in addition to Hβ for all epochs. We overlay the EW for these three emission lines in the same figure as NGC 5548. To be consistent, we utilize the continuum closest to each line. For Mg II this continuum was extracted at 3000Å while for Hβ and Hα, we use the continua at 5100Å and 6000Å respectively. We see a clear flattening behavior in Hβ in the SDSS source at higher luminosities; however, we note a rise-and-fall effect in the Balmer lines - Hα rises first, followed by Hβ. Whereas, the Mg II doesn't show any such prominent change along the luminosity trend. Not so surprisingly, the SDSS source, during its 72 epochs, modulated in Eddington ratio between (in log-scale) -0.75 to -2.5. This range is not so different from NGC 5548, which has been observed to vary in Eddington ratio between (in log-scale) -1 to -2.2. Is this a coincidence, or are we onto something? This definitely needs further investigation.

Looking into the future, we are now well-poised to utilize these findings to pre-select changing-look (and changing-state) candidates in large datasets and up-and-coming high-fidelity surveys, in conjunction with variability statistics, color-color diagrams, and marked flux variations (Shen & Burke, 2021; Ricci & Trakhtenbrot, 2023).

4. Resolving and revealing: highlights from SOAR/SIFS

Continuing our venture in the low-accretion regime, AGN spectral energy distributions (SEDs) provide a powerful diagnostic to probe the dominant ionization mechanism, test against high-quality observations, and assess the true accretion state of the AGN. In this context, we present a salient case that combines state-of-the-art photoionization modeling with one of the first high-angular-resolution integral field unit (IFU) observations obtained with the 4m SOAR

telescope. This study, focused on the nearby Seyfert 2 galaxy ESO 138-G001, directly contests earlier interpretations based on HST imaging (see Figure 5). We confirm that the observed spectra are unequivocally AGN-dominated and further demonstrate that peripheral emission structures arise from filtered radiation originating from the nucleus. Using a quantitative, iterative technique, we successfully generated synthetic spectra in remarkable agreement with both nuclear and off-nuclear observations, reinforcing the AGN-driven photoionization of this low-accreting Type-2 AGN extending beyond a few hundred parsecs from the nucleus.

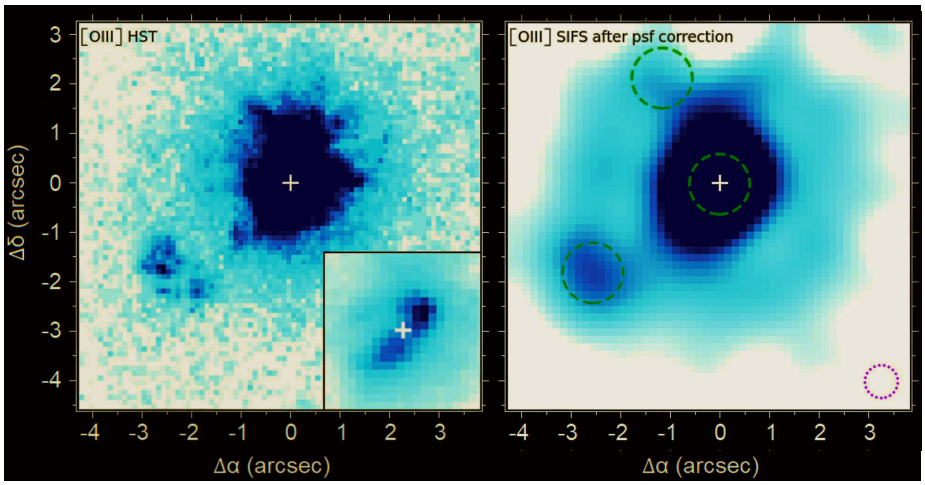

Figure 5. (*Left:*)[O III]λ5007 emission image of ESO 138-G001 from the HST/WFPC2 (Ferruit et al., 2000) with a small inset showing the details of the central part, where the nucleus is marked with a plus sign; (*Right:*) [O III]λ5007 emission image from SIFS after data treatment involving spatial re-sampling with quadratic interpolation followed by the Richardson-Lucy PSF deconvolution (see Rodríguez-Ardila et al., 2024, for more details). The green circles – with an aperture radius of 0.6 arcsec – denote the extraction regions of the spectra for the North-East (NE) knot (top left), the South-East (SE) blob (bottom left), and the nuclear region. The red circle denotes the PSF FWHM of 0.71 arcsec.

In Rodríguez-Ardila et al. (2024), we investigated the inner ∼600 pc of ESO 138-G001 using the SOAR Integral Field Spectrograph[5] (SIFS; Lepine et al. (2003)). ESO 138-G001 is the nearest known Coronal Line Forest (CLiF) AGN

[5]The SIFS IFU employs a lenslet–fiber array with 1300 elements, yielding 1300 simultaneous spectra across a 15 × 7.8 arcsec^2 field of view at a spatial sampling of 0.30 arcsec per fiber. The data span 4200–7000 Å with $R \sim 4200$.

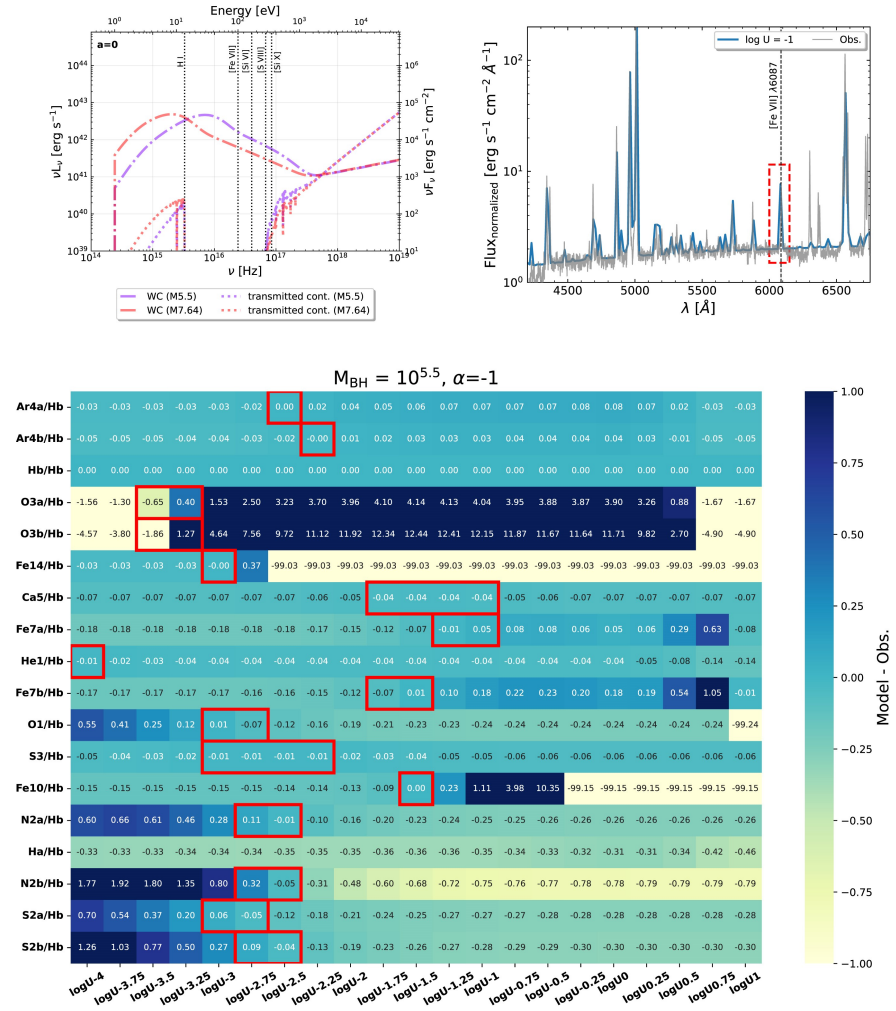

Figure 6. (*Top left:*) Incident SEDs generated for our photoionization modeling. The incident continua for the two black hole mass cases are shown in dot–dashed. These are used for the modeling of the nuclear region. The corresponding transmitted continua from these models are shown in dotted lines. These latter distributions are used as incident continua for the SE blob. These SEDs have been made assuming a non-spinning black hole. The IPs for notable coronal lines along with the hydrogen ionization front at 13.6 eV are marked with vertical lines; (*Top right:*) Synthetic spectrum (blue) comparison with observed spectrum (in grey), for the nuclear region, generated for the SED corresponding to the $M_{BH} = 10^{5.5}$ $M_{\odot}$, and ionization parameter, log U = -1. (*Bottom:*) Heatmap for the same BH mass case, $M_{BH} = 10^{5.5}$ $M_{\odot}$, for the density law slope, α = -1, for the nuclear region. Each of the considered emission lines is normalized to the Hβ emission line. The x-axis represents the range of ionization parameters considered in our models in each panel. The cases of ionization parameters for each line ratio that have the smallest residuals (modeled ratio–observed ratio) are highlighted with red boxes. Courtesy: Rodríguez-Ardila et al. (2024).

(Rose et al., 2015), characterized by unusually strong high-ionization lines (IP $\geq$ 100 eV) compared to typical AGN. This makes it an ideal laboratory to investigate the physics of coronal line emission. Earlier long-slit optical and near-infrared studies by Cerqueira-Campos et al. (2021) revealed a hidden broad-line region and a rich set of coronal lines, extending up to [Fe XIII] (IP = 330.8 eV) in the NIR.

From multiple, strong, narrow emission lines, we obtained $z = 0.00914$, corresponding to a physical scale of $\sim$146 pc arcsec^{-1}. ESO 138-G001 is notable for its compact and intense coronal line emission, as well as a bright high-excitation blob $\sim$3 arcsec southeast of the nucleus. The spatial resolution of SIFS enabled us to show that the coronal line forest emission is confined to a $\sim$0.8 arcsec region centered on the nucleus and is powered by the AGN continuum. Radiative transfer modeling further established that the AGN spectrum is filtered by circumnuclear gas within a few tens of parsecs, such that the ionization cone and the SE blob are illuminated by a modified SED dominated by low- to mid-ionization lines, with no evidence for coronal lines (Figure 6).

Photoionization modeling with `cloudy` (Ferland et al., 2017) reproduced the observed coronal line spectrum and implied a black hole mass of $\sim 3.2 \times 10^5$ $M_\odot$, consistent with the value obtained from prior X-ray variability estimates from XMM-Newton (Hernández-García et al., 2015). The inferred accretion rate is $\sim$1% of the Eddington limit. Our models recovered nearly all observed permitted and forbidden transitions, providing strong validation of the approach.

The incident SEDs were generated using the AGNSED three-component framework (disk, warm corona, hot corona; Kubota & Done 2018), which has proven effective for modeling coronal line emission across a wide range of AGN properties (Prieto et al., 2022). Applying this framework to ESO 138-G001, we leveraged its known redshift, black hole mass, and Eddington ratio to construct ionizing continua tailored to the source. While archival studies suggested discrepant mass estimates ($\log M_{BH} = 5.5$ vs. 7.64; in units of $M_\odot$), our iterative spectral synthesis confirmed the lower value, consistent with the X-ray results, and an accretion rate of $\lambda_{Edd} \approx 0.01$.

Kinematic analysis revealed broad Gaussian components in the brightest nuclear lines (e.g., [O III], Hα, [Fe VII]) with FWHM $\sim$450–600 km s^{-1}, indicative of a nuclear outflow confined within the central arcsecond. Electron densities span 10^{3-4} cm^{-3}, reaching $\sim 5.7 \times 10^3$ cm^{-3} at the nucleus, while [O III] ratios imply $T_e \sim 2.1 \times 10^4$ K. The SE blob, at $\sim$2.6 arcsec from the nucleus, displays only low- to mid-ionization lines and no coronal emission, consistent with photoionization by a filtered AGN continuum. The NE knot, in contrast, shows disturbed kinematics suggestive of interaction with a radio jet.

Taken together, these results establish ESO 138-G001 as a prototype CLiF AGN hosting a highly compact coronal line region, a modest nuclear outflow, and an ionization-cone geometry in which the SE blob and NE knot delineate the cone edges. The detailed interplay of coronal line emission, filtered radiation, and outflow/jet dynamics provides one of the clearest demonstrations to date of how AGN SEDs govern line emission in the low-accretion regime.

5. A faster, efficient way to derive masses of supermassive black holes

Let us shift gears and look into the other end of the redshift/luminosity - the high redshift, high luminosity end, which fittingly brings us to the high-Eddington sources with a relatively small increase in the black hole masses. Reverberation mapping (RM) at high redshift is notoriously time-intensive, often requiring monitoring campaigns that span decades. Landmark studies such as Lira et al. (2018) and Kaspi et al. (2021) demonstrated this challenge, as luminous quasars at $z \sim 2$–3, while ideal for RM due to their high accretion rates and massive black holes, demand prohibitively long temporal baselines. Even with decade-long surveys like LSST, obtaining reliable BLR lags for these sources remains a formidable task.

To address this, we utilized the photometric reverberation mapping (PRM) technique as a rapid, cost-effective alternative to spectroscopic RM for measuring accretion-disk (AD) sizes in high-redshift quasars via the C IV emission line (Panda et al., 2024b). Using carefully chosen medium-band filters that isolate line-free continuum regions (with $\leq$2% BLR contamination), a high-cadence monitoring campaign at the meter-class telescopes recovered rest-frame AD time delays with 10–15% precision. This method proved $\sim$166 times faster than traditional BLR-based RM (Figure 7).

Simulations based on thin-disk reprocessing ($\tau \propto \lambda^{4/3}$) coupled with high signal-to-noise ratios ($\sim$100) observations, demonstrate that modest-aperture facilities can deliver robust PRM results. The analysis yielded a radius–luminosity (R_{AD}–L_{1350}) relation with $\beta \approx 0.5$, consistent with photoionization theory. By calibrating a scaling relation between AD and BLR sizes, black-hole masses can be estimated with $\sim$23% uncertainty - an efficient alternative where direct BLR reverberation is impractical.

Building on this, Pozo Nuñez et al. (2025) demonstrated the technique during a six-month campaign of QSO J0455–4216 ($z = 2.662$), mapping an accretion disk beyond the cosmic noon for the first time. The recovered delay spectrum followed the expectations of a Shakura–Sunyaev thin disk (Shakura & Sunyaev, 1973) irradiated in a lamp-post geometry, yielding a mean emissivity radius of

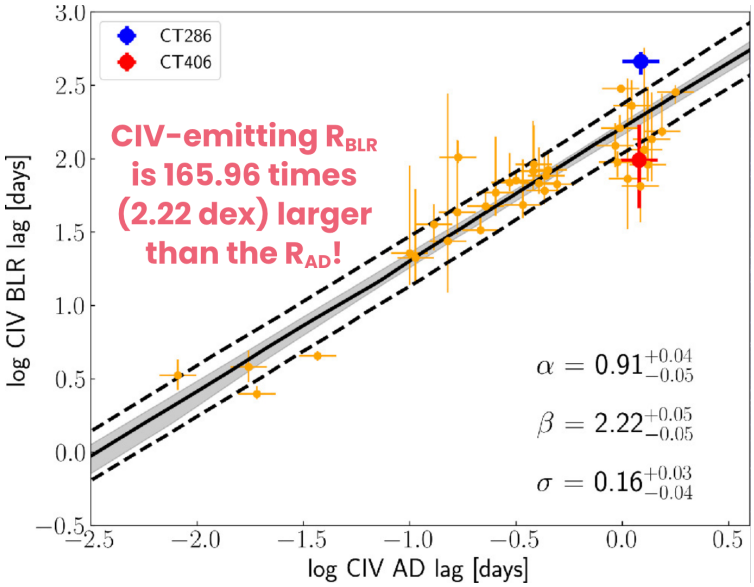

Figure 7. Recovered $R_{\rm BLR}$–$R_{\rm AD}$ relation; Courtesy: Panda et al. (2024b). The solid black line represents the mean of the posterior probability distributions, while the shaded region denotes the corresponding 1σ confidence interval. The best-fit slope (α), intercept (β), and intrinsic scatter (σ) are reported together with their 1σ uncertainties. The dashed lines indicate the mean model predictions at the upper and lower bounds when the intrinsic scatter is incorporated. The positions of the two studied sources, CT286 and CT406, which belong to the class of high-accreting sources, are marked by the blue and red circles, respectively.

$4.75^{+1.12}_{-1.05}$ light-days in the observer's frame (1.29 light-days rest frame) and implying a black hole mass of $\sim$9 $\times 10^8$ M$\odot$.

In summary, traditional C IV-based BLR lags at $z \sim 2$–3 required nearly two decades of monitoring and revealed BLR sizes corresponding to $\sim$16-year lags. In contrast, PRM can constrain AD sizes with only 4–5 months of dense monitoring, scale these to BLR sizes, and, with the aid of single-epoch spectroscopy and the virial relation, estimate black hole masses and Eddington ratios. This approach transforms the feasibility of high-redshift RM: small ground-based telescopes equipped with medium- and narrow-band filters can now probe accretion disks and black hole growth for hundreds to thousands of quasars across cosmic time, opening a rewarding avenue for future studies.

6. Why we should care about accretion-dependent SEDs and closing remarks

BHAR is straightforward to estimate; however, it depends crucially on the determination of the net bolometric output, or bolometric luminosity (L_{bol}). The estimation of the L_{bol} is not trivial and requires estimating the area under the broad-band spectral energy distribution (SED), although a crude estimate can be derived assuming a constant scaling (Richards et al., 2006) or a parametric 'bolometric correction' (Netzer, 2019) based on mean SEDs derived from composite AGN spectra. However, the overabundance of overly massive black holes at high-z (Mezcua et al., 2024; Habouzit, 2025) and them suggested to accrete at super-Eddington limits (Panda & Marziani, 2023; Marziani et al., 2025) is closely tied to our reliance on scaling relations and mean SEDs built from local samples, the latter being limited and originally made from the general population of quasars. Therefore, not only do we need accretion-dependent SEDs, but to infer bulk statistical properties of these highly-accreting AGNs and their neighborhood, we are in dire need to update our AGN SED databases, especially at higher redshifts - as we push forth to spatially resolve BLR in quasars at z=4 (GRAVITY+ Collaboration et al., 2025).

To this end, Garnica et al. (2025) presented semi-empirical spectral energy distributions (SEDs) tailored to extreme, high-accretion (xA) quasars. By integrating extensive optical survey data with multi-frequency archival data, we constructed median SEDs that capitalize on the pronounced spectral homogeneity observed among super-Eddington candidates (Panda & Marziani, 2023). The SED construction is performed in three spectral regimes - radio to NIR, optical-UV dominated by the accretion-disk, and in X-ray - each normalized at 5100Å to facilitate direct comparison with conventional templates. A systematic juxtaposition with the canonical Mathews & Ferland (MF87) SED underscores substantive divergences, particularly in the high-energy domain (see Figure 8). To evaluate the ramifications for broad-line region (BLR) diagnostics and how these SEDs affect the emitting regions, we employed `cloudy` photoionization simulations, demonstrating that the newly derived SED reproduces the extreme BLR conditions characteristic of xA quasars: markedly low ionization parameters, elevated gas densities, and supersolar metallicities. These physical conditions naturally account for the observed suppression of C IV relative to Hβ and the pronounced Fe II emission. In summary, the work delivers a data-driven, semi-empirical xA SED that diverges from traditional quasar templates and validates its influence on BLR physical-parameter determinations.

We provide `cloudy`-ready template median SED (q2) for the RQ extreme population A (drawn from the systematic analysis of 139 R_{Fe}-rich sources), along with the first and third quartiles (q1 and q3) for the community. (Garnica et al., 2025) suggests that for these xA SEDs characterized by high-to-super accretion

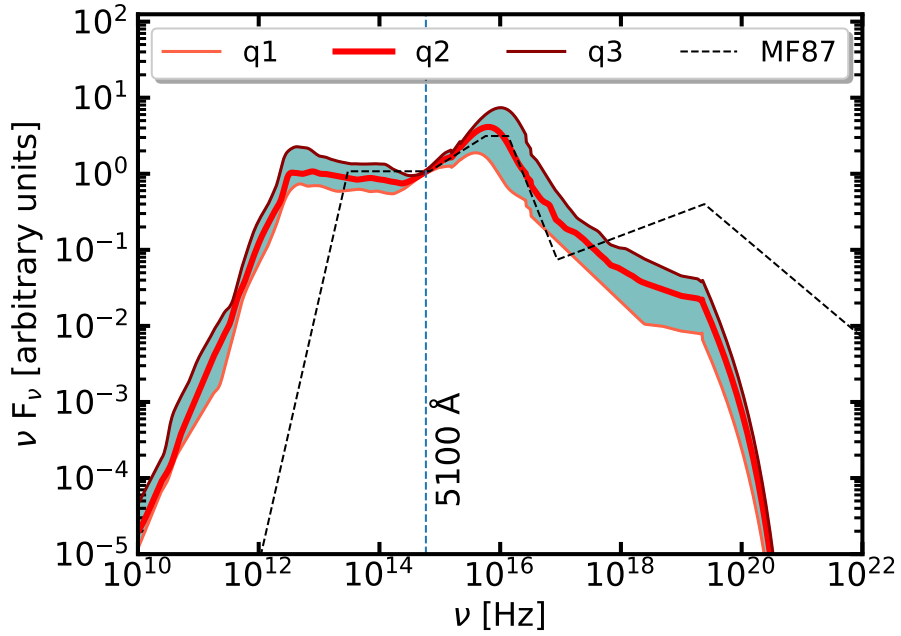

Figure 8. Spectral Energy Distributions (SEDs) from Garnica et al. (2025) for high--Eddington accreting (xA) quasars. The median SED (q2) and the inter-quartile range defined by the lower (q1) and higher (q3) SEDs are also highlighted. For reference, the often used AGN SED from Mathews & Ferland (1987) is also shown, demonstrating the variations in the broad-band SED shape relative to the Fe II strength-based SEDs.

mode, the bolometric output is more pronounced relative to the mean quasar SED from Richards et al. (2006), between 1.2 - 1.7 times higher[6].

In summary, we see that the Eddington ratio has come to our rescue in more than one way, and with the growing interest over the last decades and coming years promising more advancements and challenges, we are well-poised for many more interesting AGN-related discoveries.

Acknowledgements. S.P. is supported by the international Gemini Observatory, a program of NSF NOIRLab, which is managed by the Association of Universities for Research in Astronomy (AURA) under a cooperative agreement with the U.S. National Science Foundation, on behalf of the Gemini partnership of Argentina, Brazil, Canada, Chile, the Republic of Korea, and the United States of America. SP acknowledges the

[6]The bolometric corrections for the q1, q2 and q3 SEDs (luminosity based) are 11.16, 15.70, and 11.00, respectively.

entire organizing committee of the 15th Serbian Conference on Spectral Line Shapes in Astrophysics, for their invitation to this memorable conference. S.P. acknowledges Michael Eracleous and Ed Cackett for their helpful contributions and feedback. M.S. acknowledges support from the European Research Council (ERC) under the European Union's Horizon 2020 research and innovation program (grant agreement number 950533), and the Israel Science Foundation (grant number 1849/19). F.P.N. gratefully acknowledges the generous and invaluable support of the Klaus Tschira Foundation and funding from the European Research Council (ERC) under the European Union's Horizon 2020 research and innovation program (grant agreement No 951549).

References

Alexander, D. M., Hickox, R. C., Aird, J., et al., What drives the growth of black holes: A decade of progress. 2025, *New Astronomy Review*, **101**, 101733, DOI:10.1016/j.newar.2025.101733

Bellm, E. C., Kulkarni, S. R., Graham, M. J., et al., The Zwicky Transient Facility: System Overview, Performance, and First Results. 2019, *Publications of the ASP*, **131**, 018002, DOI:10.1088/1538-3873/aaecbe

Benati Gonçalves, H., Panda, S., Storchi Bergmann, T., Cackett, E. M., & Eracleous, M., Exploring Quasar Variability with ZTF at $0 < z < 3$: A Universal Relation with the Eddington Ratio. 2025, *Astrophysical Journal*, **988**, 27, DOI:10.3847/1538-4357/addec0

Bentz, M. C., Denney, K. D., Grier, C. J., et al., The Low-luminosity End of the Radius-Luminosity Relationship for Active Galactic Nuclei. 2013, *Astrophysical Journal*, **767**, 149, DOI:10.1088/0004-637X/767/2/149

Bentz, M. C., Peterson, B. M., Netzer, H., Pogge, R. W., & Vestergaard, M., The Radius-Luminosity Relationship for Active Galactic Nuclei: The Effect of Host-Galaxy Starlight on Luminosity Measurements. II. The Full Sample of Reverberation-Mapped AGNs. 2009, *Astrophysical Journal*, **697**, 160, DOI:10.1088/0004-637X/697/1/160

Besuner, R., Dey, A., Drlica-Wagner, A., et al., The Spectroscopic Stage-5 Experiment. 2025, *arXiv e-prints*, arXiv:2503.07923, DOI:10.48550/arXiv.2503.07923

Blandford, R. D. & McKee, C. F., Reverberation mapping of the emission line regions of Seyfert galaxies and quasars. 1982, *Astrophysical Journal*, **255**, 419, DOI:10.1086/159843

Bon, N., Bon, E., & Marziani, P., AGN Broad Line Region variability in the context of Eigenvector 1: case of NGC 5548. 2018, *Frontiers in Astronomy and Space Sciences*, **5**, 3, DOI:10.3389/fspas.2018.00003

Boroson, T. A. & Green, R. F., The Emission-Line Properties of Low-Redshift Quasi-stellar Objects. 1992, *Astrophysical Journal, Supplement*, **80**, 109, DOI:10.1086/191661

Cackett, E. M., Bentz, M. C., & Kara, E., Reverberation mapping of active galactic nuclei: from X-ray corona to dusty torus. 2021, *iScience*, **24**, 102557, DOI:10.1016/j.isci.2021.102557

Cao, S., Zajaček, M., Panda, S., et al., Standardizing reverberation-measured C IV time-lag quasars, and using them with standardized Mg II quasars to constrain cosmological parameters. 2022, *Monthly Notices of the RAS*, **516**, 1721, DOI:10.1093/mnras/stac2325

Cerqueira-Campos, F. C., Rodríguez-Ardila, A., Riffel, R., et al., Coronal-line forest active galactic nuclei - I. Physical properties of the emission-line regions. 2021, *Monthly Notices of the RAS*, **500**, 2666, DOI:10.1093/mnras/staa3320

Chelouche, D., Pozo Nuñez, F., & Kaspi, S., Direct evidence of non-disk optical continuum emission around an active black hole. 2019, *Nature Astronomy*, **3**, 251, DOI:10.1038/s41550-018-0659-x

Collin, S., Kawaguchi, T., Peterson, B. M., & Vestergaard, M., Systematic effects in measurement of black hole masses by emission-line reverberation of active galactic nuclei: Eddington ratio and inclination. 2006, *Astronomy and Astrophysics*, **456**, 75, DOI:10.1051/0004-6361:20064878

Czerny, B., Cao, S., Jaiswal, V. K., et al., Accretion disks, quasars and cosmology: meandering towards understanding. 2023a, *Astrophysics and Space Science*, **368**, 8, DOI:10.1007/s10509-023-04165-7

Czerny, B., Hryniewicz, K., Maity, I., et al., Towards equation of state of dark energy from quasar monitoring: Reverberation strategy. 2013, *Astronomy and Astrophysics*, **556**, A97, DOI:10.1051/0004-6361/201220832

Czerny, B., Panda, S., Prince, R., et al., Expectations for time-delay measurements in active galactic nuclei with the Vera Rubin Observatory. 2023b, *Astronomy and Astrophysics*, **675**, A163, DOI:10.1051/0004-6361/202345844

de Jong, R. S., Agertz, O., Berbel, A. A., et al., 4MOST: Project overview and information for the First Call for Proposals. 2019, *The Messenger*, **175**, 3, DOI:10.18727/0722-6691/5117

De Rosa, G., Peterson, B. M., Ely, J., et al., Space Telescope and Optical Reverberation Mapping Project.I. Ultraviolet Observations of the Seyfert 1 Galaxy NGC 5548 with the Cosmic Origins Spectrograph on Hubble Space Telescope. 2015, *Astrophysical Journal*, **806**, 128, DOI:10.1088/0004-637X/806/1/128

DESI Collaboration, Abdul-Karim, M., Adame, A. G., et al., Data Release 1 of the Dark Energy Spectroscopic Instrument. 2025, *arXiv e-prints*, arXiv:2503.14745, DOI:10.48550/arXiv.2503.14745

Di Valentino, E., Said, J. L., Riess, A., et al., The CosmoVerse White Paper: Addressing observational tensions in cosmology with systematics and fundamental physics. 2025, *Physics of the Dark Universe*, **49**, 101965, DOI:10.1016/j.dark.2025.101965

Drake, A. J., Djorgovski, S. G., Mahabal, A., et al., First Results from the Catalina Real-Time Transient Survey. 2009, *Astrophysical Journal*, **696**, 870, DOI:10.1088/0004-637X/696/1/870

Du, P., Lu, K.-X., Zhang, Z.-X., et al., Supermassive Black Holes with High Accretion Rates in Active Galactic Nuclei. V. A New Size-Luminosity Scaling Relation for the Broad-line Region. 2016, *Astrophysical Journal*, **825**, 126, DOI:10.3847/0004-637X/825/2/126

Du, P. & Wang, J.-M., The Radius-Luminosity Relationship Depends on Optical Spectra in Active Galactic Nuclei. 2019, *Astrophysical Journal*, **886**, 42, DOI:10.3847/1538-4357/ab4908

Du, P., Zhang, Z.-X., Wang, K., et al., Supermassive Black Holes with High Accretion Rates in Active Galactic Nuclei. IX. 10 New Observations of Reverberation Mapping and Shortened Hβ Lags. 2018, *Astrophysical Journal*, **856**, 6, DOI:10.3847/1538-4357/aaae6b

Edelson, R., Gelbord, J. M., Horne, K., et al., Space Telescope and Optical Reverberation Mapping Project. II. Swift and HST Reverberation Mapping of the Accretion Disk of NGC 5548. 2015, *Astrophysical Journal*, **806**, 129, DOI:10.1088/0004-637X/806/1/129

Fausnaugh, M. M., Denney, K. D., Barth, A. J., et al., Space Telescope and Optical Reverberation Mapping Project. III. Optical Continuum Emission and Broadband Time Delays in NGC 5548. 2016, *Astrophysical Journal*, **821**, 56, DOI:10.3847/0004-637X/821/1/56

Ferland, G. J., Chatzikos, M., Guzmán, F., et al., The 2017 Release Cloudy. 2017, *Revista Mexicana de Astronomia y Astrofisica*, **53**, 385, DOI:10.48550/arXiv.1705.10877

Ferruit, P., Wilson, A. S., & Mulchaey, J., Hubble Space Telescope WFPC2 Imaging of a Sample of Early-Type Seyfert Galaxies. 2000, *Astrophysical Journal, Supplement*, **128**, 139, DOI:10.1086/313379

Frohmaier, C., Vincenzi, M., Sullivan, M., et al., TiDES: The 4MOST Time Domain Extragalactic Survey. 2025, *arXiv e-prints*, arXiv:2501.16311, DOI:10.48550/arXiv.2501.16311

Gardner, J. P., Mather, J. C., Clampin, M., et al., The James Webb Space Telescope. 2006, *Space Science Reviews*, **123**, 485, DOI:10.1007/s11214-006-8315-7

Garnica, K., Dultzin, D., Marziani, P., & Panda, S., The spectral energy distribution of extreme population A quasars. 2025, *Monthly Notices of the RAS*, **540**, 3289, DOI:10.1093/mnras/staf862

Garnica, K., Negrete, C. A., Marziani, P., et al., High metal content of highly accreting quasars: Analysis of an extended sample. 2022, *Astronomy and Astrophysics*, **667**, A105, DOI:10.1051/0004-6361/202142837

Gaskell, C. M., Bartel, K., Deffner, J. N., & Xia, I., Anomalous broad-line region responses to continuum variability in active galactic nuclei - I. Hβ variability. 2021, *Monthly Notices of the RAS*, **508**, 6077, DOI:10.1093/mnras/stab2443

Graham, M. J., Kulkarni, S. R., Bellm, E. C., et al., The Zwicky Transient Facility: Science Objectives. 2019, *Publications of the ASP*, **131**, 078001, DOI:10.1088/1538-3873/ab006c

Graham, M. J., Ross, N. P., Stern, D., et al., Understanding extreme quasar optical variability with CRTS - II. Changing-state quasars. 2020, *Monthly Notices of the RAS*, **491**, 4925, DOI:10.1093/mnras/stz3244

GRAVITY+ Collaboration, El Dayem, K. A., Aimar, N., et al., Spatially resolved broad line region in a quasar at z=4: Dynamical black hole mass and prominent outflow. 2025, *arXiv e-prints*, arXiv:2509.13911, DOI:10.48550/arXiv.2509.13911

Grier, C. J., Trump, J. R., Shen, Y., et al., The Sloan Digital Sky Survey Reverberation Mapping Project: Hα and Hβ Reverberation Measurements from First-year Spectroscopy and Photometry. 2017, *Astrophysical Journal*, **851**, 21, DOI:10.3847/1538-4357/aa98dc

Guo, H., Shen, Y., & Wang, S. 2018, PyQSOFit: Python code to fit the spectrum of quasars, Astrophysics Source Code Library, record ascl:1809.008

Guo, W.-J., Pan, Z., Siudek, M., et al., The First Identification of Lyα Changing-look Quasars at High Redshift in DESI. 2025a, *Astrophysical Journal, Letters*, **981**, L8, DOI:10.3847/2041-8213/adb426

Guo, W.-J., Zou, H., Greenwell, C. L., et al., Changing-look Active Galactic Nuclei from the Dark Energy Spectroscopic Instrument. II. Statistical Properties from the First Data Release. 2025b, *Astrophysical Journal, Supplement*, **278**, 28, DOI:10.3847/1538-4365/adc124

Haas, M., Chini, R., Ramolla, M., et al., Photometric AGN reverberation mapping - an efficient tool for BLR sizes, black hole masses, and host-subtracted AGN luminosities. 2011, *Astronomy and Astrophysics*, **535**, A73, DOI:10.1051/0004-6361/201117325

Habouzit, M., Is the JWST detecting too many AGN candidates? 2025, *Monthly Notices of the RAS*, **537**, 2323, DOI:10.1093/mnras/staf167

Hernández-García, L., Masegosa, J., González-Martín, O., & Márquez, I., X-ray spectral variability of Seyfert 2 galaxies. 2015, *Astronomy and Astrophysics*, **579**, A90, DOI:10.1051/0004-6361/201526127

Ivezić, Ž., Kahn, S. M., Tyson, J. A., et al., LSST: From Science Drivers to Reference Design and Anticipated Data Products. 2019, *Astrophysical Journal*, **873**, 111, DOI:10.3847/1538-4357/ab042c

Jaiswal, V. K., Mandal, A. K., Prince, R., et al., Application of the FRADO model of BLR formation to the Seyfert galaxy NGC 5548 and the first step toward determining the Hubble constant. 2024, *arXiv e-prints*, arXiv:2410.03597, DOI:10.48550/arXiv.2410.03597

Kaspi, S., Brandt, W. N., Maoz, D., et al., Taking a Long Look: A Two-decade Reverberation Mapping Study of High-luminosity Quasars. 2021, *Astrophysical Journal*, **915**, 129, DOI:10.3847/1538-4357/ac00aa

Kaspi, S., Smith, P. S., Netzer, H., et al., Reverberation Measurements for 17 Quasars and the Size-Mass-Luminosity Relations in Active Galactic Nuclei. 2000, *Astrophysical Journal*, **533**, 631, DOI:10.1086/308704

Klimek, E. S., Gaskell, C. M., & Hedrick, C. H., Optical Variability of Narrow-Line Seyfert 1 Galaxies. 2004, *Astrophysical Journal*, **609**, 69, DOI:10.1086/420809

Kollmeier, J., Anderson, S. F., Blanc, G. A., et al., SDSS-V Pioneering Panoptic Spectroscopy. 2019, *Bulletin of the American Astronomical Society*, **51**, 274

Kubota, A. & Done, C., A physical model of the broad-band continuum of AGN and its implications for the UV/X relation and optical variability. 2018, *Monthly Notices of the RAS*, **480**, 1247, DOI:10.1093/mnras/sty1890

Lepine, J. R. D., de Oliveira, A. C., Figueredo, M. V., et al., SIFUS: SOAR integral field unit spectrograph. 2003, in Society of Photo-Optical Instrumentation Engineers (SPIE) Conference Series, Vol. **4841**, *Instrument Design and Performance for Optical/Infrared Ground-based Telescopes*, ed. M. Iye & A. F. M. Moorwood, 1086–1095

Lira, P., Kaspi, S., Netzer, H., et al., Reverberation Mapping of Luminous Quasars at High z. 2018, *Astrophysical Journal*, **865**, 56, DOI:10.3847/1538-4357/aada45

Mainieri, V., Anderson, R. I., Brinchmann, J., et al., The Wide-field Spectroscopic Telescope (WST) Science White Paper. 2024, *arXiv e-prints*, arXiv:2403.05398, DOI:10.48550/arXiv.2403.05398

Martínez-Aldama, M. L., Czerny, B., Kawka, D., et al., Can Reverberation-measured Quasars Be Used for Cosmology? 2019, *Astrophysical Journal*, **883**, 170, DOI:10.3847/1538-4357/ab3728

Martínez-Aldama, M. L., Panda, S., Czerny, B., et al., The CaFe Project: Optical Fe II and Near-infrared Ca II Triplet Emission in Active Galaxies. II. The Driver(s) of the Ca II and Fe II and Its Potential Use as a Chemical Clock. 2021, *Astrophysical Journal*, **918**, 29, DOI:10.3847/1538-4357/ac03b6

Marziani, P., Dultzin, D., Sulentic, J. W., et al., A main sequence for quasars. 2018, *Frontiers in Astronomy and Space Sciences*, **5**, 6, DOI:10.3389/fspas.2018.00006

Marziani, P., Garnica Luna, K., Floris, A., et al., Super-Eddington Accretion in Quasars. 2025, *Universe*, **11**, 69, DOI:10.3390/universe11020069

Marziani, P. & Sulentic, J. W., Highly accreting quasars: sample definition and possible cosmological implications. 2014, *Monthly Notices of the RAS*, **442**, 1211, DOI:10.1093/mnras/stu951

Marziani, P., Sulentic, J. W., Zamanov, R., et al., An Optical Spectroscopic Atlas of Low-Redshift Active Galactic Nuclei. 2003a, *Astrophysical Journal, Supplement*, **145**, 199, DOI:10.1086/346025

Marziani, P., Sulentic, J. W., Zwitter, T., Dultzin-Hacyan, D., & Calvani, M., Searching for the Physical Drivers of the Eigenvector 1 Correlation Space. 2001, *Astrophysical Journal*, **558**, 553, DOI:10.1086/322286

Marziani, P., Zamanov, R. K., Sulentic, J. W., & Calvani, M., Searching for the physical drivers of eigenvector 1: influence of black hole mass and Eddington ratio. 2003b, *Monthly Notices of the RAS*, **345**, 1133, DOI:10.1046/j.1365-2966.2003.07033.x

Mathews, W. G. & Ferland, G. J., What Heats the Hot Phase in Active Nuclei? 1987, *Astrophysical Journal*, **323**, 456, DOI:10.1086/165843

Mezcua, M., Pacucci, F., Suh, H., Siudek, M., & Natarajan, P., Overmassive Black Holes at Cosmic Noon: Linking the Local and the High-redshift Universe. 2024, *Astrophysical Journal, Letters*, **966**, L30, DOI:10.3847/2041-8213/ad3c2a

Negrete, C. A., Dultzin, D., Marziani, P., & Sulentic, J. W., Reverberation and Photoionization Estimates of the Broad-line Region Radius in Low-z Quasars. 2013, *Astrophysical Journal*, **771**, 31, DOI:10.1088/0004-637X/771/1/31

Netzer, H., Revisiting the Unified Model of Active Galactic Nuclei. 2015, *Annual Review of Astron and Astrophys*, **53**, 365, DOI:10.1146/annurev-astro-082214-122302

Netzer, H., Bolometric correction factors for active galactic nuclei. 2019, *Monthly Notices of the RAS*, **488**, 5185, DOI:10.1093/mnras/stz2016

Noda, H. & Done, C., Explaining changing-look AGN with state transition triggered by rapid mass accretion rate drop. 2018, *Monthly Notices of the RAS*, **480**, 3898, DOI:10.1093/mnras/sty2032

Osterbrock, D. E. & Ferland, G. J. 2006, *Astrophysics of gaseous nebulae and active galactic nuclei*

Padovani, P., Alexander, D. M., Assef, R. J., et al., Active galactic nuclei: what's in a name? 2017, *Astronomy and Astrophysics Reviews*, **25**, 2, DOI:10.1007/s00159-017-0102-9

Panda, S., Parameterizing the AGN Radius–Luminosity Relation from the Eigenvector 1 Viewpoint. 2022, *Frontiers in Astronomy and Space Sciences*, **9**, 850409, DOI:10.3389/fspas.2022.850409

Panda, S., Unveiling the quasar main sequence: illuminating the complexity of active galactic nuclei and their evolution. 2024, *Frontiers in Astronomy and Space Sciences*, **11**, 1479874, DOI:10.3389/fspas.2024.1479874

Panda, S., Bon, E., Marziani, P., & Bon, N., Taming the derivative: Diagnostics of the continuum and Hβ emission in a prototypical Population B active galaxy. 2022, *Astronomische Nachrichten*, **343**, e210091, DOI:10.1002/asna.20210091

Panda, S., Bon, E., Marziani, P., & Bon, N., Saturation of the curve: Diagnostics of the continuum and Hβ emission in Population B active galaxy NGC 5548. 2023, *Bulletin of the Astronomical Society of Brazil*, **34**, 246, DOI:10.48550/arXiv.2308.05831

Panda, S., Kozłowski, S., Gromadzki, M., et al., Virial Black Hole Masses for Active Galactic Nuclei behind the Magellanic Clouds. 2024a, *Astrophysical Journal, Supplement*, **272**, 11, DOI:10.3847/1538-4365/ad3549

Panda, S., Martínez-Aldama, M. L., & Zajaček, M., Current and future applications of Reverberation-mapped quasars in Cosmology. 2019a, *Frontiers in Astronomy and Space Sciences*, **6**, 75, DOI:10.3389/fspas.2019.00075

Panda, S. & Marziani, P., High Eddington quasars as discovery tools: current state and challenges. 2023, *Frontiers in Astronomy and Space Sciences*, **10**, 1130103, DOI:10.3389/fspas.2023.1130103

Panda, S., Marziani, P., & Czerny, B., The Quasar Main Sequence Explained by the Combination of Eddington Ratio, Metallicity, and Orientation. 2019b, *Astrophysical Journal*, **882**, 79, DOI:10.3847/1538-4357/ab3292

Panda, S., Pozo Nuñez, F., Bañados, E., & Heidt, J., Probing the C IV Continuum Size–Luminosity Relation in Active Galactic Nuclei with Photometric Reverbera-

tion Mapping. 2024b, *Astrophysical Journal, Letters*, **968**, L16, DOI:10.3847/2041-8213/ad5014

Panda, S. & Śniegowska, M., Changing-look Active Galactic Nuclei. I. Tracking the Transition on the Main Sequence of Quasars. 2024, *Astrophysical Journal, Supplement*, **272**, 13, DOI:10.3847/1538-4365/ad344f

Pei, L., Fausnaugh, M. M., Barth, A. J., et al., Space Telescope and Optical Reverberation Mapping Project. V. Optical Spectroscopic Campaign and Emission-line Analysis for NGC 5548. 2017, *Astrophysical Journal*, **837**, 131, DOI:10.3847/1538-4357/aa5eb1

Peterson, B. M., Berlind, P., Bertram, R., et al., Steps toward Determination of the Size and Structure of the Broad-Line Region in Active Galactic Nuclei. XVI. A 13 Year Study of Spectral Variability in NGC 5548. 2002, *Astrophysical Journal*, **581**, 197, DOI:10.1086/344197

Peterson, B. M., Denney, K. D., De Rosa, G., et al., The Size of the Narrow-line-emitting Region in the Seyfert 1 Galaxy NGC 5548 from Emission-line Variability. 2013, *Astrophysical Journal*, **779**, 109, DOI:10.1088/0004-637X/779/2/109

Peterson, B. M., Ferrarese, L., Gilbert, K. M., et al., Central Masses and Broad-Line Region Sizes of Active Galactic Nuclei. II. A Homogeneous Analysis of a Large Reverberation-Mapping Database. 2004, *Astrophysical Journal*, **613**, 682, DOI:10.1086/423269

Pozo Nuñez, F., Bañados, E., Panda, S., & Heidt, J., Accretion disc reverberation mapping in a high-redshift quasar. 2025, *Astronomy and Astrophysics*, **700**, L8, DOI:10.1051/0004-6361/202555421

Pozo Nuñez, F., Bruckmann, C., Deesamutara, S., et al., Modelling photometric reverberation mapping data for the next generation of big data surveys. Quasar accretion discs sizes with the LSST. 2023, *Monthly Notices of the RAS*, **522**, 2002, DOI:10.1093/mnras/stad286

Pozo Nuñez, F., Czerny, B., Panda, S., et al., Reevaluating LSST's Capability for Time Delay Measurements in Quasar Accretion Disks. 2024, *Research Notes of the American Astronomical Society*, **8**, 47, DOI:10.3847/2515-5172/ad284a

Prieto, A., Rodríguez-Ardila, A., Panda, S., & Marinello, M., A novel black hole mass scaling relation based on coronal gas, and its dependence with the accretion disc. 2022, *Monthly Notices of the RAS*, **510**, 1010, DOI:10.1093/mnras/stab3414

Pronik, V. I. & Chuvaev, K. K., Hydrogen lines in the spectrum of the galaxy Markaryan 6 during its activity. 1972, *Astrophysics*, **8**, 112, DOI:10.1007/BF01002159

Pucha, R., Juneau, S., Dey, A., et al., Tripling the Census of Dwarf AGN Candidates Using DESI Early Data. 2025, *Astrophysical Journal*, **982**, 10, DOI:10.3847/1538-4357/adb1dd

Ren, W., Wang, J., Cai, Z., & Guo, H., Extreme Variability Quasars in Their Various States. I. The Sample Selection and Composite SDSS Spectra. 2022, *Astrophysical Journal*, **925**, 50, DOI:10.3847/1538-4357/ac3828

Ricci, C. & Trakhtenbrot, B., Changing-look active galactic nuclei. 2023, *Nature Astronomy*, **7**, 1282, DOI:10.1038/s41550-023-02108-4

Richards, G. T., Lacy, M., Storrie-Lombardi, L. J., et al., Spectral Energy Distributions and Multiwavelength Selection of Type 1 Quasars. 2006, *Astrophysical Journal, Supplement*, **166**, 470, DOI:10.1086/506525

Rodríguez-Ardila, A., May, D., Panda, S., Fonseca-Faria, M. A., & Fraga, L., The narrow-line region properties of ESO 138-G001 unveiled by SOAR/SIFS observations. 2024, *Monthly Notices of the RAS*, **527**, 10649, DOI:10.1093/mnras/stad3872

Rose, M., Elvis, M., & Tadhunter, C. N., Coronal-Line Forest AGN: the best view of the inner edge of the AGN torus? 2015, *Monthly Notices of the RAS*, **448**, 2900, DOI:10.1093/mnras/stv113

Ross, N. P., Graham, M. J., Calderone, G., et al., The first high-redshift changing-look quasars. 2020, *Monthly Notices of the RAS*, **498**, 2339, DOI:10.1093/mnras/staa2415

Sánchez-Sáez, P., Lira, H., Martí, L., et al., Searching for Changing-state AGNs in Massive Data Sets. I. Applying Deep Learning and Anomaly-detection Techniques to Find AGNs with Anomalous Variability Behaviors. 2021, *Astronomical Journal*, **162**, 206, DOI:10.3847/1538-3881/ac1426

Shakura, N. I. & Sunyaev, R. A., Black holes in binary systems. Observational appearance. 1973, *Astronomy and Astrophysics*, **24**, 337

Shapovalova, A. I., Doroshenko, V. T., Bochkarev, N. G., et al., Profile variability of the Hα and Hβ broad emission lines in NGC 5548. 2004, *Astronomy and Astrophysics*, **422**, 925, DOI:10.1051/0004-6361:20035652

Shen, Y. & Burke, C. J., A Sample Bias in Quasar Variability Studies. 2021, *Astrophysical Journal, Letters*, **918**, L19, DOI:10.3847/2041-8213/ac1e2e

Shen, Y. & Ho, L. C., The diversity of quasars unified by accretion and orientation. 2014, *Nature*, **513**, 210, DOI:10.1038/nature13712

Shen, Y., Richards, G. T., Strauss, M. A., et al., A Catalog of Quasar Properties from Sloan Digital Sky Survey Data Release 7. 2011, *Astrophysical Journal, Supplement*, **194**, 45, DOI:10.1088/0067-0049/194/2/45

Sniegowska, M., Czerny, B., Bon, E., & Bon, N., Possible mechanism for multiple changing-look phenomena in active galactic nuclei. 2020, *Astronomy and Astrophysics*, **641**, A167, DOI:10.1051/0004-6361/202038575

Śniegowska, M., Marziani, P., Czerny, B., et al., High Metal Content of Highly Accreting Quasars. 2021, *Astrophysical Journal*, **910**, 115, DOI:10.3847/1538-4357/abe1c8

Suganuma, M., Yoshii, Y., Kobayashi, Y., et al., Reverberation Measurements of the Inner Radius of the Dust Torus in Nearby Seyfert 1 Galaxies. 2006, *Astrophysical Journal*, **639**, 46, DOI:10.1086/499326

Sulentic, J. W., Marziani, P., & Dultzin-Hacyan, D., Phenomenology of Broad Emission Lines in Active Galactic Nuclei. 2000, *Annual Review of Astron and Astrophys*, **38**, 521, DOI:10.1146/annurev.astro.38.1.521

Temple, M. J., Ricci, C., Koss, M. J., et al., BASS XXXIX: Swift-BAT AGN with changing-look optical spectra. 2023, *Monthly Notices of the RAS*, **518**, 2938, DOI:10.1093/mnras/stac3279

Vestergaard, M. & Peterson, B. M., Determining Central Black Hole Masses in Distant Active Galaxies and Quasars. II. Improved Optical and UV Scaling Relationships. 2006, *Astrophysical Journal*, **641**, 689, DOI:10.1086/500572

Wandel, A., On the Baldwin Effect in Active Galactic Nuclei. I. The Continuum-Spectrum-Mass Relationship. 1999, *Astrophysical Journal*, **527**, 649, DOI:10.1086/308134

Wandel, A., Peterson, B. M., & Malkan, M. A., Central Masses and Broad-Line Region Sizes of Active Galactic Nuclei. I. Comparing the Photoionization and Reverberation Techniques. 1999, *Astrophysical Journal*, **526**, 579, DOI:10.1086/308017

Wang, J., Xu, D. W., & Wei, J. Y., Identification of SDSS J141324.27+530527.0 as a New "Changing-look" Quasar with a "Turn-on" Transition. 2018, *Astrophysical Journal*, **858**, 49, DOI:10.3847/1538-4357/aab88b

Wang, S., Woo, J.-H., Gallo, E., et al., Identifying Changing-look AGNs Using Variability Characteristics. 2024, *Astrophysical Journal*, **966**, 128, DOI:10.3847/1538-4357/ad3049

Watson, D., Denney, K. D., Vestergaard, M., & Davis, T. M., A New Cosmological Distance Measure Using Active Galactic Nuclei. 2011, *Astrophysical Journal, Letters*, **740**, L49, DOI:10.1088/2041-8205/740/2/L49

Wu, Q. & Shen, Y., A Catalog of Quasar Properties from Sloan Digital Sky Survey Data Release 16. 2022, *Astrophysical Journal, Supplement*, **263**, 42, DOI:10.3847/1538-4365/ac9ead

Zeltyn, G., Trakhtenbrot, B., Eracleous, M., et al., Exploring Changing-look Active Galactic Nuclei with the Sloan Digital Sky Survey V: First Year Results. 2024, *Astrophysical Journal*, **966**, 85, DOI:10.3847/1538-4357/ad2f30